GROWTH OF MECHANICALLY GENERATED WAVES UNDER A FOLLOWING WIND, I

NIZUNO, Shinjiro
Research Institute for Applied Mechanics, Kyushu University: Assistant Professor

https://doi.org/10.5109/7173514

出版情報：Reports of Research Institute for Applied Mechanics. 22 (71), pp.357-376, 1975. 九州大学応用力学研究所
バージョン：
権利関係：

Reports of Research Institute for Applied Mechanics
Vol. XXII, No. 71, 1975

GROWTH OF MECHANICALLY GENERATED WAVES UNDER A FOLLOWING WIND, I

By Shinjiro MIZUNO*

An experimental investigation has been made to study the growth process of regular waves generated mechanically under the action of the wind. Principal emphasis is given to the description of the wave field of strong nonlinear interactions which occur after waves have reached the limiting steepness as well as to the wave growth. Waves are measured at seven stations at an interval of about 1.2 m along the test section, and the wave energy and power spectra are computed. The wave period used is short (0.4-0.7 sec), and the wind speed ranges from 2.5 to 10 m/s. Waves first grow exponentially. The measured wave growth is about 1.5 times as great as the Miles prediction, about a half of that of Bole & Hsu, lies roughly along the Snyder & Cox line, and further is of the same order of magnitude as the attenuation of the waves propagating against the wind for the low speed below 10 m/s. The shortest waves of period 0.4 sec reach the limiting steepness at the middle of the test section, at which stage they become unstable, break up into random waves, and finally grow up into more developed wind-waves than usual. At the same time, energy is transferred from the fundamental frequency of regular waves toward slightly lower frequencies by strong nonlinear interactions.

1. Introduction

In this paper we study experimentally the development of regular waves generated mechanically under the influence of the wind. For convenience' sake, the development of waves is devided into two stages.

In the first stage waves grow exponentially. The wave growth in this stage has been considerably well studied by many investigators for comparison with the Miles [1] linear instability theory. Among other things, in the laboratory measurements of wave elevation and wave-induced pressure fluctuations, Shemdin & Hsu [2] estimated energy and momentum flux from air to waves of the same order as the Miles prediction. In a later experiment, however, Bole & Hsu [3] made a detailed measurement of the growth of mechanically generated waves under the influence of the wind as a function of fetch and obtained the growth rate about 3 times greater than predicted by Miles. In the ocean, Snyder & Cox [4] measured the growth rate of a single wave component (17 m) by towing an array of wave recorders down-

*Assistant Professor, Research Institute for Applied Mechanics, Kyushu University, Fukuoka, Japan.

wind at the group velocity of the component, and found that the wave growth was almost an order of magnitude greater than predicted by Miles. The field experiment by Barnett & Wilkerson[5] also confirmed that the observed growth was consistent with that of Snyder & Cox. Most of the experimental results are quantitatively considerably greater than the Miles prediction, except for the study of Shemdin & Hsu[2].

In the second stage, mechanically generated waves reach the maximum steepness, at which they break up, and the wave field is governed by nolinear interactions such as wave breaking, conservative wave-wave interactions formulated by Hasselmann[6], and so on. As far as the author knows, the growth mechanism in this range has never in detail studied up to the present. Perhaps Hasselman's nonlinear energy transfer theory will be very efficient for the understanding of the evolution process in this range. Recently in the JONSWAP experiment, Hasselmann *et al*[7]. computed nonlinear energy transfer rates for a number of spectral shapes of wind waves, and found that nonlinear interactions played a predominant role in controlling the shape of the spectrum and its evolution from short to long waves.

The present study is the first step to realize the second range of development within the wave tank by making the period of waves as short as possible and to examine the physical mechanism of the transition process of mechanically generated waves from regular to wind waves.

2. Experimental Apparatus and Data Analysis

Experiments were made in a wind wave tunnel 80 cm high, 60 cm wide and with a usable test section length of 850 cm. Depth of the water and air were 35 and 45 cm, respectively. Fig. 1 shows an outlook of the experimental apparatus used in this experiment. The air was sucked through the tunnel by a centrifugal type of blower downwind of the test section, and made uniform by honeycombs and a number of fine mesh screens, before it entered the section. To thicken the boundary layer, a roughned transition plate was installed at the air inlet. The bottom of the transition plate was 5 cm above the water surface to maintain sufficient clearlence for mechani-

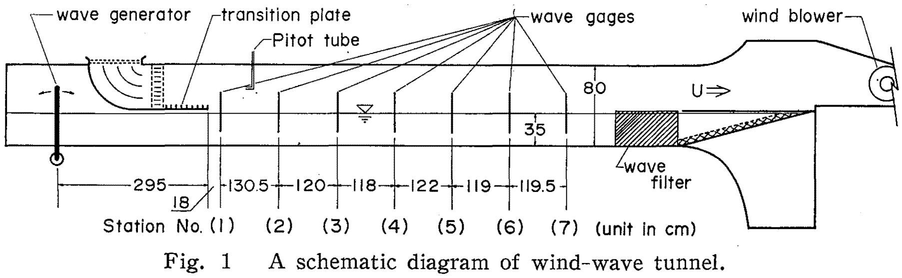

Fig. 1 A schematic diagram of wind-wave tunnel.

cally generated waves of largest amplitude. A sloping beach of wooden plate covered with scrubbing-brushes and wave filters of wire gauzes were situated downwind of the test section, to absorb wave energy.

Measurements of waves were made simultaneously at seven stations of measurement with resistance-type wave gauges each of which uses a parallel platinum wire of 0.1 mm diameter. The stations of measurement were arranged at an interval of approximately 120 cm along the test section, as shown in Fig. 1. Vertical wind velocity profiles were measured at four stations (Stations No. 2, the middle point of No. 2, and No. 3, No. 4, and No. 6), using a standard Pitot static tube, and a reference air velocity U_r was measured at the position of a uniform velocity profile 25 cm above the water and 50 cm from the tip of the transition plate.

Since most of energy of wind waves in our laboratory experiment is contained in the frequency components less than 10 Hz and the sampling rate must be more than twice the maximum frequency of the analysis, we choose the Nyquist frequency of 12.5 Hz and a sampling rate of 25 Hz. The spectral analysis was made on a YHP-2100 mini-computer which had an 8-channel A-D converter. As the core size of the mini-computer was small, we splitted a time series into several sets of segments which consisted of 256 data points, and made a harmonic analysis for each segment, using the fast Fourier transform (FFT) procedure. The discrete Fourier transform is defined by

$$C(k)=\frac{1}{N}\sum_{t=0}^{N-1}X(t)\exp(-2\pi ikt/N) \qquad k=0, \cdots\cdots, (N-1) \tag{1}$$

where $C(k)$ is the k th complex coefficient of the discrete Fourier transform and $X(t)$ denotes the t th sample of the time series which consists of N sample points. Then we obtain a raw power spectral dencity $\phi(f_k)$

$$\phi(f_k)=2N\Delta t\cdot|C(k)|^2, \qquad k=1,\ 2, \cdots\cdots,\ \frac{N}{2} \tag{2}$$

where f_k is $k/N\Delta t$ and Δt the time interval of sampling.

From the statistical theory of spectral estimation, when the time series is normal, $\phi(f_k)$ is independently distributed as χ^2 variables with 2 degrees of freedom. This means that in no statistical sense dose $\phi(f_k)$ converse to a smooth power spectral distribution when N becomes large. In order to improve the spectral estimates, it is reasonable to take an ensemble mean of those raw power spectral density distributions. Thus we obtain improved power spectral density

$$<\phi(f_k)>=\frac{1}{M}\sum_{m=1}^{M}\phi_m(f_k) \qquad k=1, \cdots\cdots, \frac{N}{2} \tag{3}$$

where the variance of $<\phi(f_k)>$ is approximately given by M times that of raw spectra $\phi(f_k)$. In order to obtain more smooth power spectral distribution, it is desirable to apply the hanning window to $<\phi(f_k)>$.

Now we attempt to obtain enegy of regular waves from the above power spectra. If we consider a sinusoidal wave of $X(t)=A\exp(2\pi i\frac{l}{N}t)$, then $C(k)$ is exactly given by

$$C(k)=A\frac{\sin\pi(l-k)}{N\sin\frac{\pi}{N}(l-k)}\exp\{i\pi(N-1)\frac{(l-k)}{N}\}, \tag{4}$$

and its power spectra $\phi(f_k)$ by

$$\phi(f_k)=2A\Delta t\frac{\sin^2\pi(l-k)}{N\sin^2\frac{\pi}{N}(l-k)} \tag{5}$$

This means that if l is any positive integer below $N/2$, the FFT is perfect, but that if l is no integer, then every $\phi(f_k)$ will be affected. This is known as "leakage effect". It follows that the enegy of regular waves will in general distribute over every spectral line, even if it is really a single spectral line. Since, however, most of the energy is centered at several spectral lines in the neighbourhood of the frequency l, as is evident from eq. (5), we assume that the energy of regular waves is approximately given by the sum of a central peak line plus two of its both side as follows:

$$E=\Delta f\cdot[<\phi(f_{p-1})>+<\phi(f_p)>+<\phi(f_{p+1})>]. \tag{6}$$

As far as a sinusoidal wave is concerned, the energy loss calculated by eq. (6) is at most 15% of the true energy.

3. Experimental Results and Discussion

3.1. Velocity Profiles

Air velocity profiles over the water surface were measured at four stations (St. 2, between 2 and 3, 4 and 6) for the cases of wind waves alone, and of the coexistence system of wind waves and mechanically generated waves of period 0.4 and 0.7 sec under the air speed of 5 to 10 m/sec. Logarithmic velocity distributions were quite well fitted to the measured data in the boundary layer above the water surface. Hence, values of U_* and Z_0 were calculated by applying each set of the wind data to the logarithmic law,

$$\frac{U}{U_*}=\frac{1}{\kappa}\ln(\frac{Z}{Z_0}). \tag{7}$$

where U is the mean velocity at the height Z above the water surface at rest, U_* the friction velocity of the wind, Z_0 the roughness parameter, and κ the Von Karman constant $(=0.4)$. All of the results are listed in Table 1, and only U_* is plotted against fetch in Fig. 2. It is seen that only for the

Table 1 Characteristics of air flow above water.

U_r (m/s)	wave period (sec)	station 2		middle point of 2 & 3		station 4		station 6	
		U_* (cm/s)	$Z_0 \times 10^3$ (cm)	U_* (cm/s)	$Z_0 \times 10^3$ (cm)	U_* (cm/s)	$Z_0 \times 10^3$ (cm)	U_* (cm/s)	$Z_0 \times 10^3$ (cm)
5.0	wind wave	10.8	0.004	14.8	0.03	21.7	1.3	24.1	2.8
	0.4	—	—	—	—	20.8	0.91	20.2	0.58
	0.7	—	—	—	—	24.3	2.68	26.0	5.4
7.5	wind wave	23.9	0.2	28.7	0.61	40.4	7.43	42.9	12.2
	0.4	—	—	29.5	0.87	39.5	6.03	42.2	10.6
	0.7	—	—	—	—	38.5	5.25	42.0	10.3
10.0	wind wave	37.8	1.0	46.9	4.6	57.2	12.2	60.8	16.9
	0.4	—	—	46.5	4.4	71.2	43.0	75.1	65.6
	0.7	—	—	58.6	17.9	60.2	16.2	58.1	26.0

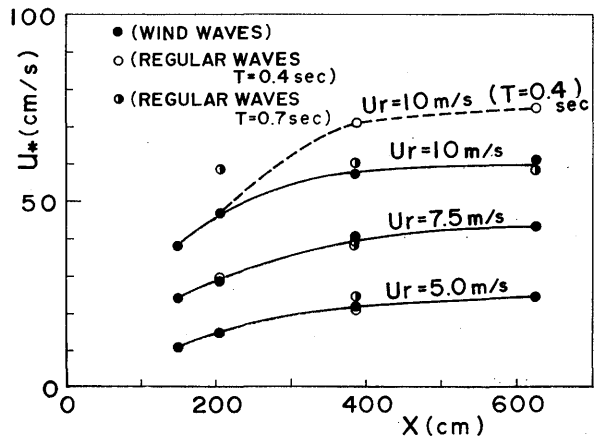

Fig. 2 The friction velocity U_* obtained from the mean velocity profile measurements over the water surface.

case of waves of period 0.4 sec for the air speed of 10 m/s, U_* is significantly affected by the presence of mechanically generated waves in the region between Station No. 4 and No. 6. This increase of U_* seems to be associated with the breaking of mechanically generated waves, because the wave breaking brings about the formation of rough water surface including local flow separation, and the increase of the wind stress over water (cf. **3.3**).

3.2. Growth Rate of Regular waves

We first attempt to study the growth process of regular waves generated by a wave generator under the influence of a following wind. From a preliminary test, it was found that when the waves entered the wind area,

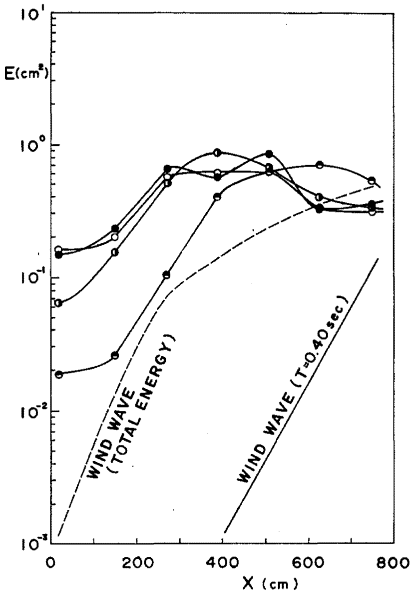

(a) U_r=10 m/sec. T=0.4 sec; wave No. 1, ◒; No. 2, ◑; No. 3, ●, No. 4, ○.

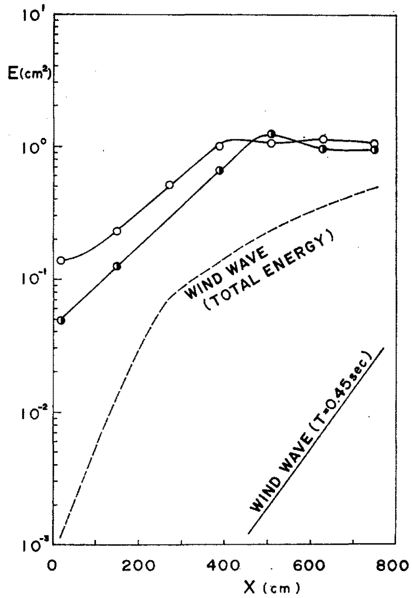

(b) U_r=10 m/sec, T=0.45 sec; No. 5, ◑; No. 6, ○.

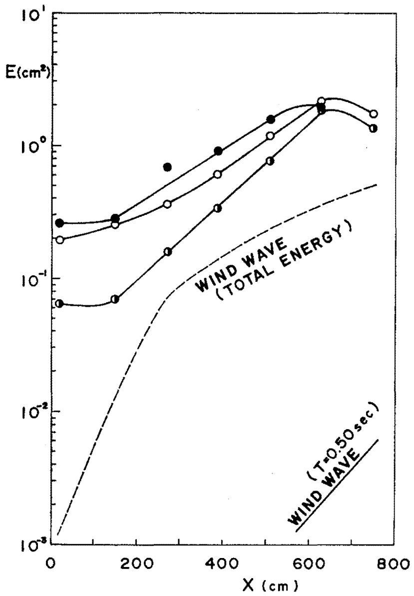

(c) U_r=10 m/sec, T=0.5 sec; No. 7, ◑; No. 8, ○; No, 9, ●.

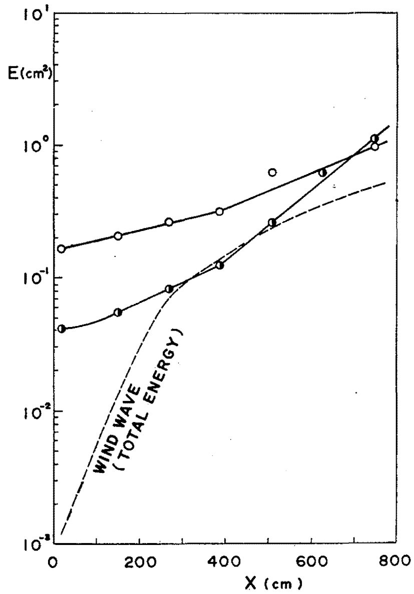

(d) U_r=10 m/sec, T=0.59 sec; No. 10, ◑; No. 11, ○.

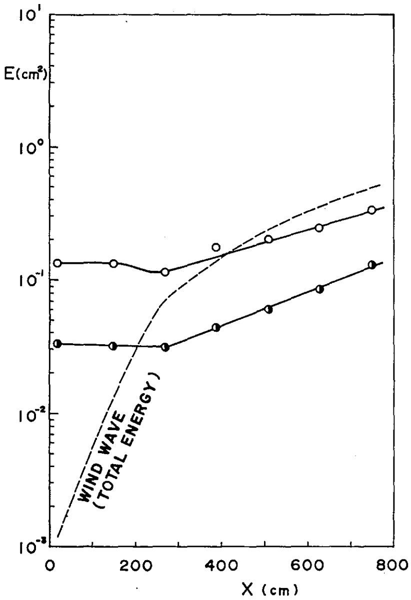

(e) U_r=10m/sec, T=0.7 sec;
No. 12, ◑; No. 13, ○.

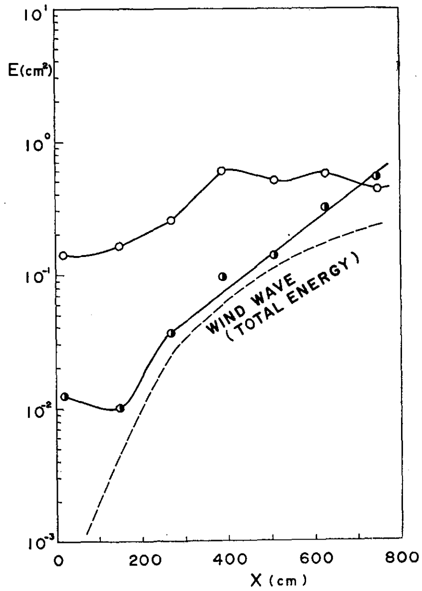

(f) U_r=7.5 m/sec, T=0.4 sec;
No. 14, ◑; No. 15, ○.

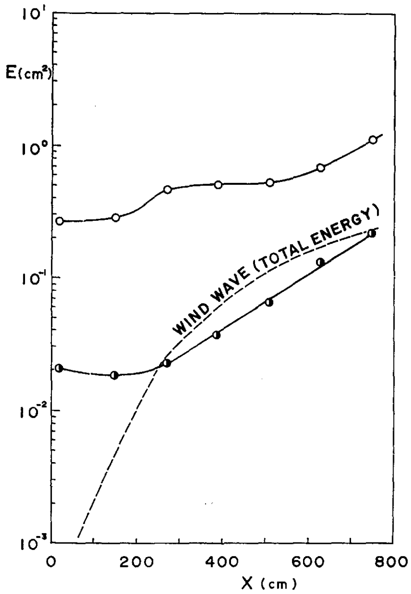

(g) U_r=7.5 m/sec, T=0.5 sec;
No. 16, ◑; No. 17, ○,

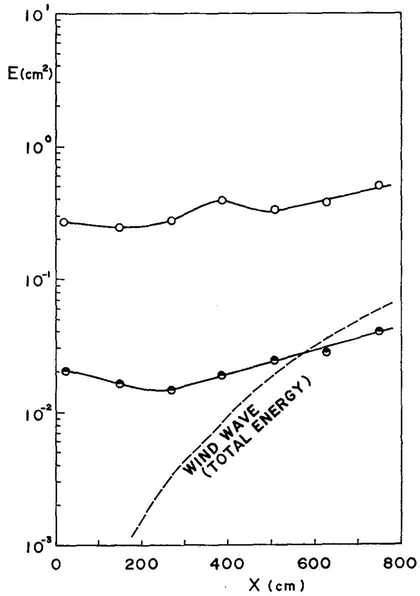

(h) U_r=5.0 m/sec, T=0.5 m/sec;
No. 18◓; No. 19, ○.

Fig. 3 The development of the energy of the fundamental frequency of mechanically generated waves under a following wind, cf. Table 2.

they first decayed over several wave lengths and subsequently developed with the fetch. Therefore, in order to realize the growth process of the waves within the wave tank, it was necessary to make wave period as short as possible, so that the wave period from 0.4 to 0.7 sec were used in this experiment. Mean velocity of air above the water surface was changed from 2.5 to 10 m/sec in steps. The measurement of wave was made for three minutes two minutes after the wave generator had operated under a constant air velocity. Fig. 3 shows the development of regular wave trains as a function of the fetch, where the energy of regular waves (E) was calculated from the fundamental frequency components of the power spectra of waves measured at each station, according to the way mentioned in the previous section. Higher harmonics of regular waves are not included in E, because the contribution of higher harmonics is negligibly small, i.e. 5% at most. The total and the corresponding component energy of wind waves under the same condition are also indicated in Fig. 3 for comparison with the growth of regular waves. For example, we can see that the energy of regular waves was much greater than that of wind waves for the wave data

Table 2 The growth rates of waves.

Wave No.	U_r (m/sec)	T (sec)	L_0 (cm)	C_0 (cm/sec)	H_1 (cm)	U_* (cm/sec)	$\alpha(\mathrm{cm}^{-1}) \times 10^3$	ε_0	Reference
1	10.0	0.4	25.0	62.4	0.39	46.9	11.6	0.29	Fig. 3(a)
2					0.72		10.2	0.255	
3					1.09		7.10	0.177	
4					1.14		8.58	0.214	
5	10.0	0.45	31.6	72.0	0.63	46.9	7.04	0.222	Fig. 3(b)
6					1.06		6.48	0.205	
7	10.0	0.5	39.0	78.0	0.72	57.2	6.73	0.262	Fig. 3(c)
8					1.25		5.28	0.206	
9					1.45		4.74	0.185	
10	10.0	0.59	55.0	93.2	0.57	57.2	3.26~6.23	0.179~0.342	Fig. 3(d)
11					1.15		1.72~3.14	0.095~0.172	
12	10.0	0.7	76.0	108.6	0.52	57.2	2.92	0.222	Fig. 3(e)
13					1.04		2.24	0.170	
14	7.5	0.4	25.0	62.4	0.31	40.4	5.62~9.21	0.140~0.230	Fig. 3(f)
15					1.07		3.66~7.61	0.091~0.190	
16	7.5	0.5	39.0	78.0	0.41	41.0	4.8	0.187	Fig. 3(g)
17					1.46		3.1	0.122	
18	5.0	0.5	39.0	78.0	0.40	21.7	2.03	0.079	Fig. 3(h)
19					1.47		1.7	0.066	

of Fig. 3 (a)−(c).

Regions of exponential growth are indicated by the straight portions of each curve, from which the growth rate of waves has been calculated and listed in Table 2, where the spatial growth rate α and nondimensional growth rate ε_0 are defined as follows:

$$E=E_0\exp(\alpha X)=E_0\exp(\varepsilon_0\cdot X/L_0) \tag{8}$$

where L_0 is the wave length determined from wave period using small amplitude wave theory. On comparing the growth rates among the waves of the same period and reference air velocity, they agreed rather well with each other, but it was found that they depended slightly on the wave amplitude of the station 1, H_1. Fig. 4 shows how the growth rate ε_0 changes with H_1 for the wave data of air velocity of 10 m/sec with the wave period as a parameter. It is seen that it decreases with increasing H_1 for the waves of the same period. Its cause seems to be an interaction between regular waves and drift current which occurs near the inlet of air folw. In our laboratory experiment regular waves are generated in a calm air region by a wave generator. Then, a steady non-uniform horizontal surface current must arise just downstream of the transition plate, because there is no current below the transition plate but the wind produces drift current as well as wind waves downstream of it. A theoretical investigation of Longuet-

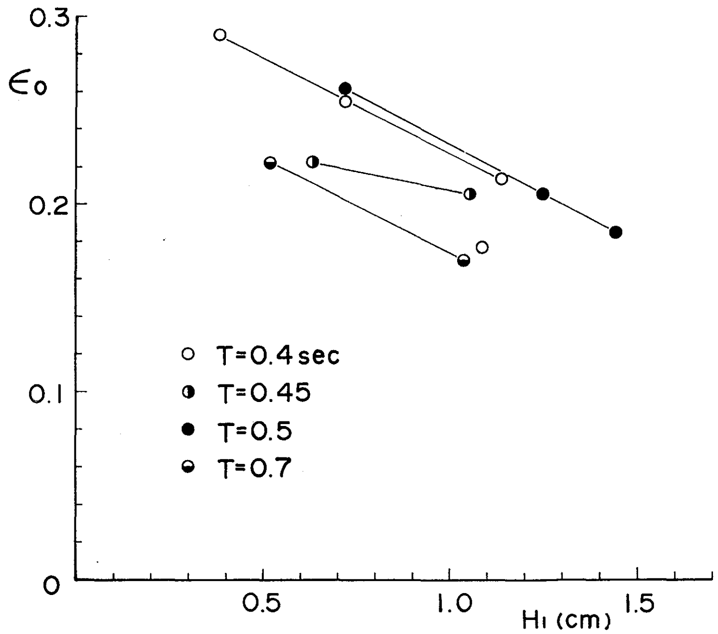

Fig. 4 The dependence of the growth rates ε_0 on the amplitude H_1 of incident waves, ($U_r=10$ m/sec).

Higgins & Stewarts[8] predicts that when mechanically generated waves come across such a steady non-uniform current, an interchange of energy occurs between waves and current by the radiation stress effects, which in the present situation cause the wave attenuation just downstream of the transition plate. This theory qualitatively explains the wave attenuation obserbed at the early stage of development of mechanically generatad waves. It seems to be natural that the same mechanism has an effect on the wave growth, if it occurs near the transition plate. As is evident from the growth curve of Fig. 3, the growth region of mechnically generated waves shifts to the left, i. e. to the negative direction of the X-axis with increasing the amplitude H_1 of waves at station 1. This means that the growth rates for a higher wave height H_1 should be more affected by the attenuation action due to the interaction between waves and current than those for a lower one.

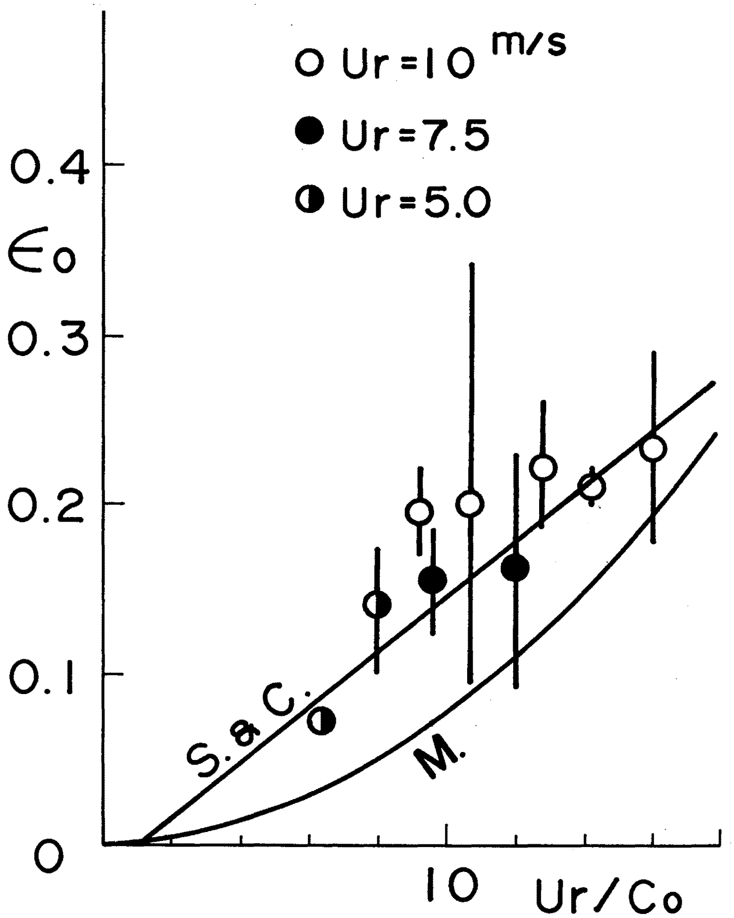

Fig. 5 The growth rate ε_0 of the wave energy against U_r/C_0 in a following wind.

Now all the growth rates obtained are plotted against U_r/C_0 in Fig. 5. Snyder & Cox empirical relation and Miles theory of invicid laminar model are also indicated in Fig. 5 for comparison with the experimental values. Snyder & Cox obtained the following best fitted relation to fit their measurements of wave growth in the sea:

$$\beta=\frac{\rho_a}{\rho_w}(kU-\omega) \tag{9}$$

where ρ_a and ρ_w are density of air and water respectively, k is wave number, ω angular frequency and β is growth rate of wave energy with time. Using the relation $x=\frac{1}{2}C_0t$, where $1/2C_0$ is the group velocity of waves, it is converted into the spatial growth rate ε_0 as follows:

$$\varepsilon_0=\frac{\beta}{2f}=\pi\frac{\rho_a}{\rho_w}(U/C_0-1). \tag{10}$$

For Miles curve we assumed $\beta_M=3$, where β_M indicates the imaginary part of a dimensionless pressure coefficient used by Miles, since the critical height $Z_c=0.01\sim0.02$ and $\xi_c=kZ_c\approx2\times10^3$. Furthermore, from experimental results, U_r is equal to $20\,U^*$ within the limit of 15%. The experimental values lie roughly along the Snyder & Cox line and about 1.5 times greater than the Miles curve, although they are very scattered.

Bole & Hsu measured the growth rates of mechanically generated waves of period between 0.7 and 1.1 sec for air velocity of 3.6 to 13.2 m/sec. They list only the ratio of the experimental to Miles theoretical growth rates, so that a direct comparison of their experimental values with ours is impossible. Their conclusion is that the experimental values are greater than Miles theoretical values by a factor varying from 1 to 10, with a mean of about 3. Thus, the Bole & Hsu data seem to be about twice greater than ours. A better agreement, however, is seen with ours for the Bole & Hsu data whose experimental conditions agree approximately with ours, that is, for the data of wave periods between 0.7 and 0.9 sec and of blower revolution number of 250 and 300 r.p.m.

In a previous experiment we also examined the attenuation of mechanically generated waves in an adverse wind condition. Fig. 6 and 7 show the attenuation rates ε_0 of height of mechanically generated waves against the wind as a function of U_r/C_0 and U_*/C_0, respectively. Before making a comparison with the present data, we should make some remarks. The experimental values of Fig. 5 must be compared with twice those of Fig. 6 and 7, since the wave energy is proportional to the square of the wave height. The experimental conditions are somewhat different in both experiments. The main difference is that wave periods used in the adverse wind condition were between 0.8 and 1.2 second and considerably higher than those in the present one.

In comparing Fig. 5 with Fig. 6, we find that the dimensionless growth and attenation rates are of the same order of magnitude if U_r/C_0 is less than 10, but that for further higher U_r/C_0, the attenuation rates are much higher than the growth rates. Fig. 9 (a) shows an example of the net source function $S(f)$ in the exponentially growing region of waves, where $S(f)$ yields the enegy transfer across the frequencies in the growing process of waves. It is evident from Fig. 9 (a) that the wave growth occurs predominantly at the fundamental frequency (2.5 Hz) of the waves.*

Hence, nonlinear wave-wave interactions will be very weak even if it occurs, so that a greater part of the wave growth is due to the energy input from the wind. This confirms the growth of a linear type of surface waves. If this is the case, it is surprising that our growth rates of waves lie approximately along the Snyder & Cox line, because in the JONSWAP experiments it was shown that a greater part of the growth rate on the forward face of the spectrum of wind waves was attributed to the nonlinear

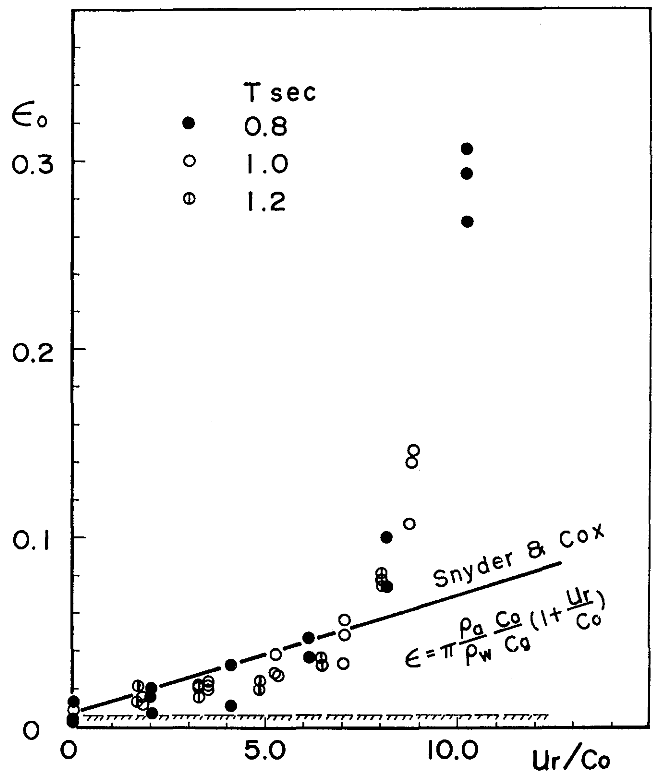

Fig. 6 The attenuation rate ε_0 of the wave amplitude against U_r/C_0 in an adverse wind.

*The broadening of the line of the net source function across the frequencies is not essential, because it is mainly due to the spectral window at the data analysis.

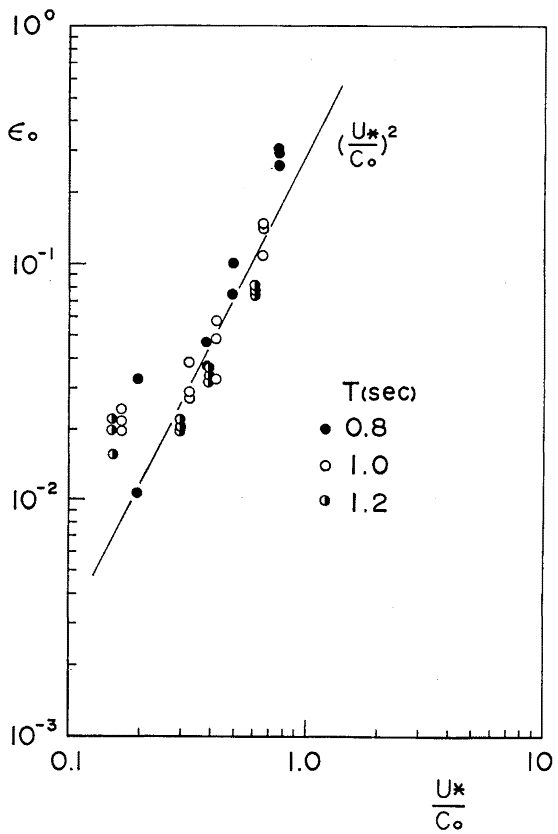

Fig. 7 The attenuation rate ε_0 of the wave amplitude against U_r/C_0 in an adverse wind.

energy transfer across the spectrum. In order to clarify the physical mechanism of the growth or attenuation of waves, a further study is necessary to obtain the direct energy input from the wind to the waves. Fig. 7 shows another way of plotting the attenuation coefficients. This way of representation may be more appropriate for the experimental data of the attenuation coefficients, but while the same way was applied to the data of the present growth rates, we could not always obtain good results.

3.3. Growth process all over the wave tank

In the previous paragraph we focused attention on the growth rates of mechanically generated waves. In this paragraph we consider the development of mechanically generated waves all over the fetch under a following wind. Mechanically generated waves can not continue to grow infinitely in a following wind; As the wave steepness increases, they become unstable

Table 3 The maximum height and steepness of waves, where $L_b=1.2\ L_0$.

Wave No.	U_r (m/sec)	Station	T (sec)	L_b (cm)	Number of waves	H_{max} (cm)	$H_{1/10}$ (cm)	$H_{1/3}$ (cm)	H_{mean} (cm)	H_{max}/L_b	$H_{1/10}/L_b$	$H_{1/3}/L_b$	H_{mean}/L_b
1	10	6	0.4	30.0	151	5.37	4.42	3.92	2.99	0.179	0.147	0.131	0.100
2	10	4	0.4	30.0	149	4.07	3.86	3.56	2.89	0.136	0.129	0.119	0.096
3	10	5	0.4	30.0	151	5.28	4.76	4.35	3.42	0.176	0.159	0.145	0.114
4	10	5	0.4	30.0	149	5.09	4.38	3.85	2.98	0.170	0.146	0.128	0.099
5	10	5	0.45	37.9	145	6.26	5.65	5.19	4.19	0.165	0.149	0.137	0.110
6	10	6	0.45	37.9	146	4.91	4.58	4.28	3.53	0.130	0.121	0.113	0.093
7	10	6	0.5	46.8	148	6.44	5.80	5.33	4.67	0.138	0.124	0.114	0.100
8	10	6	0.5	46.8	149	5.94	5.51	5.17	4.64	0.127	0.118	0.110	0.099
9	10	6	0.5	46.8	148	5.87	5.56	5.19	4.59	0.125	0.119	0.111	0.098

and finally reach the limit of the wave breaking. In fact, among the mechanically generated waves measured, the waves of longer period continued to grow monotonously in the range of the wave tank except for the early stage of development, but after some ones of shorter period continued to grow exponentially, they reached a maximum amplitude somewhere in the wave tank, as shown in Fig. 3 (a) — 3 (c). We first examine the maximum wave steepness for the waves whose amplitude reached a maximum within the wave tank.

According to Michell theory, the maximum steepness corresponding to the Stokes criterion for wave breaking in deep water is

$$(H_b/L_b)_{max}=0.142$$

where L_b is the finite amplitude wave length at which breaking occurs in deep water, and 1.2 times the wavelength L_0 from small amplitude wave theory (see Ippen *et al.*[9)]). For comparison with the Michell theory, the maximum wave steepness based on H_{max}, $H_{1/3}$, $H_{1/10}$ and H_{mean}, respectively, representing the maximum height, and the average height of the highest one tenth, the highest one third, and all the waves, was calculated from about 150 wave trains at the station of the maximum value of the energy E of Fig. 3, and listed in Table 3. It is found that the maximum wave steepness based on $H_{1/10}$ agrees approximately with the Michell theoretical value, although the maximum steepness of longer period has a tendency to be slightly less than the theoretical value even for the experimental data of H_{max}/L_b.

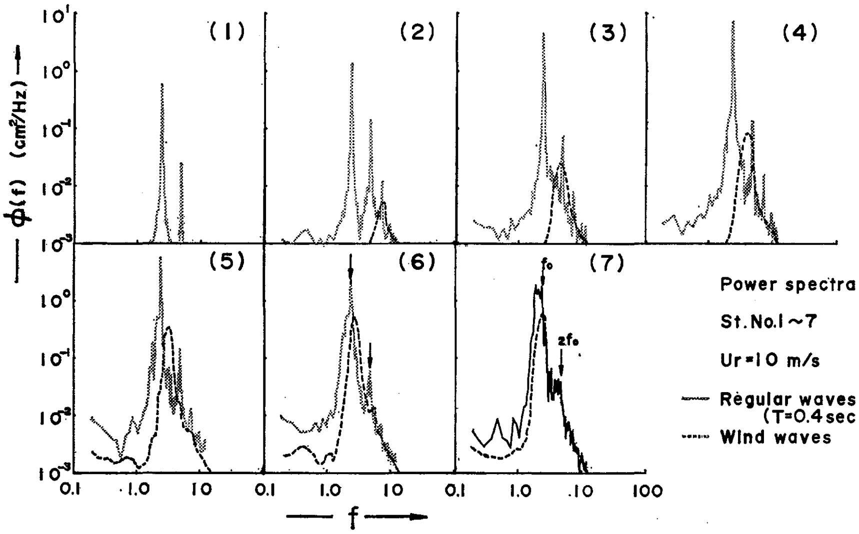

Fig. 8 The comparison of the power spectra between wind waves and mechanically generated waves (wave No. 2).

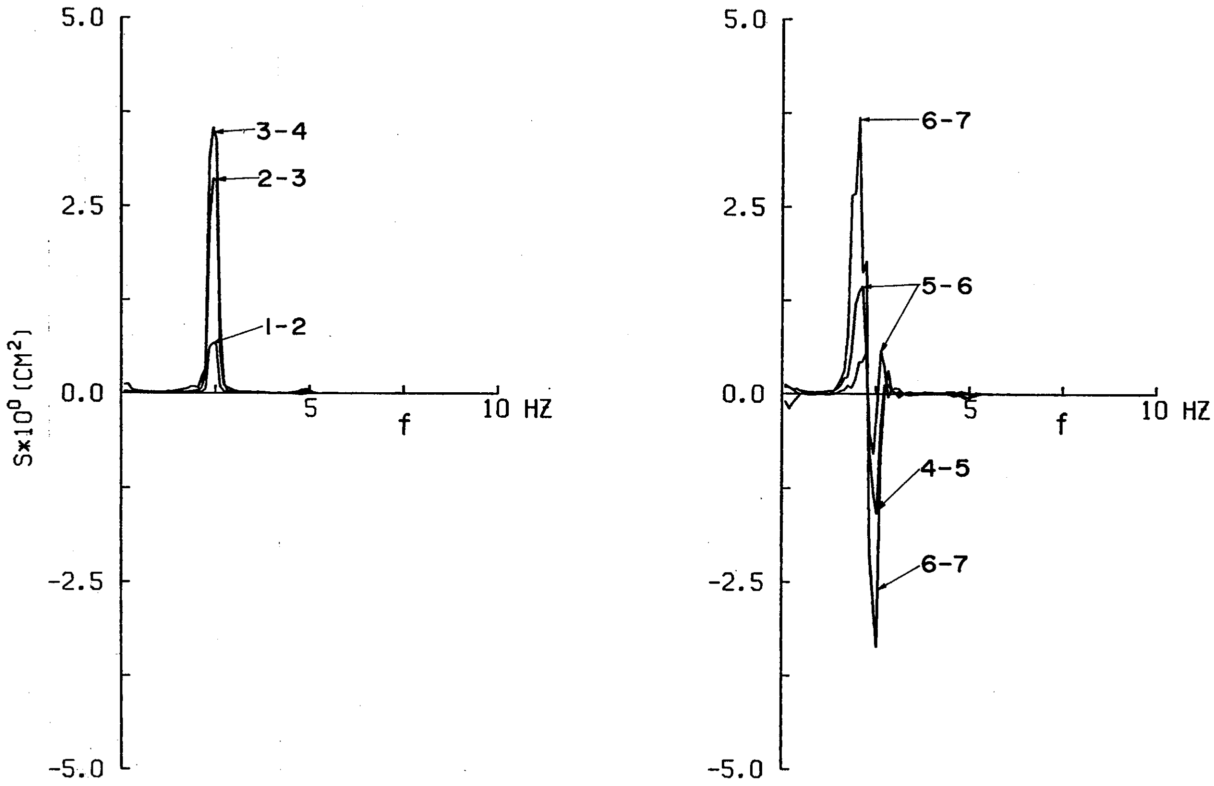

(a) exponentially growing stage (b) transition stage.

Fig. 9 Net source function S computed from the spectra of the waves (No. 2) at two adjacent stations.

As mentioned above, if we make the period of mechanically generated waves as short as possible, they grow rapidly in the direction of the wind and come to have the maximum wave steepness in the middle section of the tank. In fact, the wave train (wave No. 2, cf. Table 2) of period 0.4 sec and height H_1 0.7 cm, which was one of the shortest waves that could be generated, reached the maximum amplitude at station 4 about 3.5 m from the air inlet in an air velocity of 10 m/sec. We now attempt to examine in some detail how this wave train develops all over the wave tank.

The evolution of the wave train is shown in Fig. 8, 9 and 10 as a function of fetch, where Fig. 8 gives power spectral density distributions $\phi(f)$, Fig. 9 the net source functions $S(f)$, which have been already defined in 3.2, and Fig. 10 total energy E_{total} of the wave train, E, which is energy of the fundamenal component of the mechanically generated waves, and E_L and E_H, which are energies of lower and higher frequency components than the fundamental, respectively, where $E_{total}=E_L+E+E_H$. An inspection of those figures suggests that it is appropriate to distinguish the whole range of the wave tank into two different ones:

1) The range of station 1 to 4. The wave growth at this range will be termed to be at "exponentially growing stage".

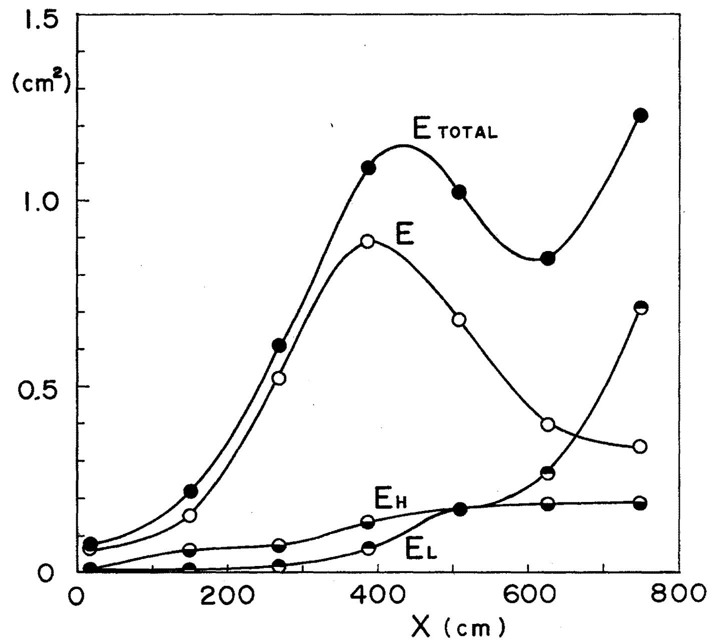

Fig. 10 The development of energy of the waves (No. 2). E_{total}, the total energy; E, the fundamental component; E_L, the lower frequency components; E_H; the higher ones, where $E_{total}=E_L+E+E_H$.

2) The range of station 4 to 7. The wave growth at this range will be termed to be at "transition stage".

At the exponentially growing stage, the power spectral distributions of the wave train (Figs. 8(1)−8(4)) are characterized by a sharp spectral peak and higher harmonics, and the energy imput from air directly caused the spectral peak to develop without change of shape. Fig. 9 (a) more clearly shows that the wave growth is predominant only at the spectral peak.

At the transition stage, the sharp spectral peak no longer grows but rather attenuates. One of the most characteristic features is a drastic change of spectral structure of mechanically generated waves through the transition stage. That is, the power spectrum gradually changes from a sharp to broad band spectrum, as shown by the thin dotted line in Fig. 8 (4) −8 (7). The power spectrum of Fig. 8 (7) is again shown in Fig. 11, and

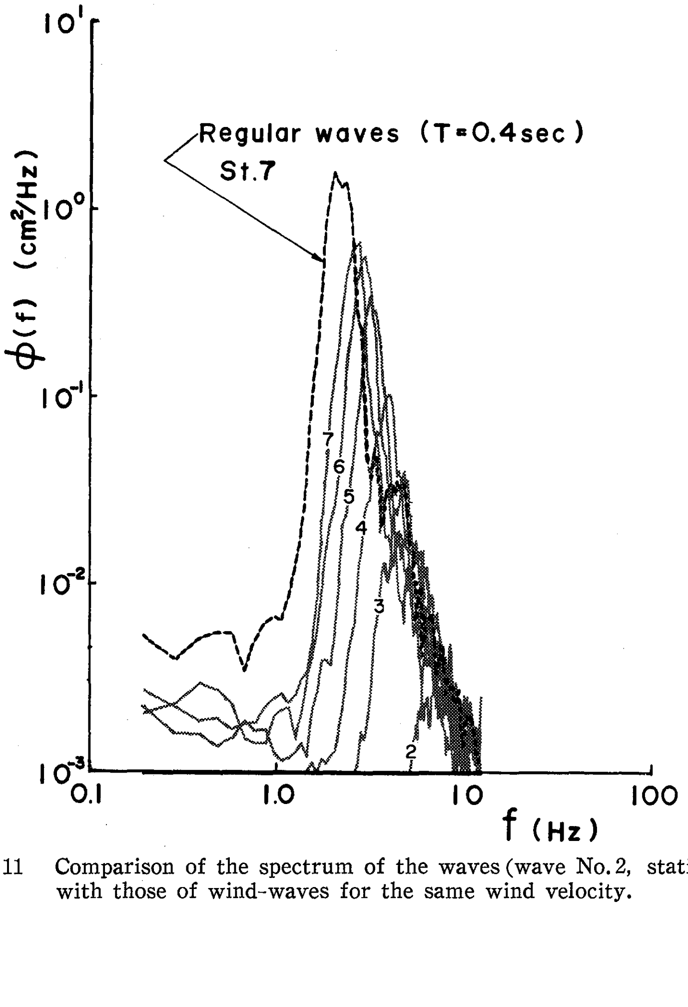

Fig. 11 Comparison of the spectrum of the waves (wave No. 2, station 7) with those of wind-waves for the same wind velocity.

compared with those of wind waves alone, which were generated under the same wind velocity. It is clear by comparison that the power spectrum of mechanically generated waves finally comes to have a spectral structure, which is very similar to that of fetch-limited wind waves, and that the development of the former is in a more developed stage than that of wind waves alone under the same air velocity.

The second characteristic feature is the energy transfer across the power spectrum. This seems to be due to the situation that the peak frequency in the power spectrum of wind waves (the broken line in Fig. 8) approaches to the fundamental frequency of regular waves (the thin dotted line in Fig. 8) with the increase of fetch, and that a greater part of both spectra lies on each other at the transition stage. Energy is transferred from the fundamental frequency (2.5 Hz) of the regular waves to slightly lower ones, as is evident from the net source functions $S(f)$ in Fig. 9 (*b*), which are characterized by a positive lobe corresponding to the wave growth of slightly lower components than the spectral peak and a negative lobe corresponding to the wave attenuation directly beneath the spectral peak. The energy transfer is roughly estimated also from the two curves of E and E_L in Fig. 10. The energy transfer described here may be at least qualitatively explained by the nonlinear energy transfer theory due to conservative wave-wave interactions formulated by Hasselmann. Actually, it should be noted that the function shape of $S(f)$ in Fig. 9 (b) has a surprisingly close resemblance to that of the nonlinear energy transfer term, which was calculated for "the sharp spectrum" in the JONSWAP experiments made by Hasselmann *et al.*

The third characteristic feature of the transition stage is the wave breaking. There appears a region where the total energy E_{total} of waves slightly decreases in the development process of waves, as shown in Fig. 10. The attenuation of the total energy clearly means that a considerably greater energy dissipation than energy input from the wind occurs by the wave breaking. As mentioned before, the waves of period 0.4 sec become sufficiently steep to reach the limiting steepness at station 4. They, of course, are long-crested there. By visual observation, these long-crested regular waves seem to split into a number of random short-crested waves through the transition stage. If it is the case, it is reasonable to consider that strong nonlinear interactions are brought about by the breaking of long-crested waves into short-crested waves due to the instability of water surface by both the limiting steepness and the strong wind shear stress. Actually, we have already pointed out the occurence of the limiting steepness (cf. Table 3) and the increase of the friction velocity U_*(cf. Fig. 2) at the transition stage. It is evident that such a breaking process is accompanied by a great energy dissipation and little energy input from the wind, because both the wave field and pressure fluctuations above the water surface would be more random and incoherent than usual. This is the reason why the total energy of waves should decrease at the transition stage.

Up to now, we have discussed only the waves of the shortest period measured. Although the similar phenomenon could not be observed for other waves of longer period, we believe that if the wave tank were longer, we could come accross the same phenomenon for those waves. However, there might be another possibility that nonlinear interactions between wind waves and mechanically generated waves occur before the latter have reached the limiting steepness.

In summary, the whole picture of the development of mechanically generated waves under the influence of the wind is as follows: Mechanically generated waves of a constant period first grow exponentially and almost independently of local wind waves, until they reach a limiting steepness predicted by the Stokes criterion of wave breaking, at which stage they become unstable, break up into random short-crested waves, and at the same time the energy of the fundamental component of regular waves is transferred toward slightly lower frequencies by non-linear wave-wave interactions, and finally grow up into more developed wind waves than usual.

Acknowledgements

The author wishes to express his gratitude to Professor H. Mitsuyasu for many valuable discussions and for his interest and support during this investigation. He is also indebted to the co-operation of both Mr. K. Eto and Mr. M. Tanaka in carrying out this experiment, and to Miss N. Uraguchi for typing of the manuscript.

References

1) Miles, J. W., On the generation of surface waves by shear flows, J. Fluid Mech., Vol. 3, 1957, pp. 185-204.
2) Shemdin, O. H. and Hsu, E. Y., The dynamics of wind in the vicinity of progressive water waves, J. Fluid Mech., Vol. 30, 1966, pp. 403-416.
3) Bole, J. B. and Hsu, E. Y., Response of gravity water waves to wind excitation, J. Fluid Mech., Vol. 35, 1969, pp. 657-675.
4) Snyder, R. L. and Cox, C. S., A field study of the wind generation of ocean waves, J. Mar. Res., Vol. 24, 1966, pp. 141-178.
5) Barnett, T. P. and Wilkerson, J. C., On the generation of wind waves as inferred from airborne rader measurements of fetch-limited spectra, J. Mar. Res., Vol. 25, 1967, pp. 292-328.
6) Hasselmann, K., On the non-linear energy transfer in a gravity-wave spectrum, Part 1., J. Fluid Mech., Vol. 12, pp. 481-500.
7) Hasselmann, K., Barnett, T. P., Bouws, E., Carlson, H., Cartwright, D. E., Enke, K., Ewing, J. A., Gienapp, H., Hasselmann, D. E., Krusemann, P., Meerburg, A., Müller, P., Olbers, D. J., Richter, K., Sell, W. and Walden, H., Measurements of wind-wave growth and swell decay during the joint North Sea Wave Project (JONSWAP), Erganzungsheft zur Deutschen Hydrographischen Zeitschrift, Reihe A (8), Nr. 12, 1973.
8) Longuet-Higgins, M. S. and Stewart, R. W., The changes in amplitude of short gravity waves on steady non-uniform currents, J. Fluid Mech., Vol. 10, 1961, pp. 529-549.
9) Ippen, A. T,. Editor: Estuary and Coastline Hydrodynamics, Engineering Societies Monographs, McGRAW-HILL B. C., Chapter 2, Finite amplitude waves, 1966, pp. 93-132.

(Recieved November, 30, 1974)